EXPERIMENTAL STUDY ON VELOCITY-PRESSURE CORRELATION IN TURBULENT MIXING LAYER OUT OF EQUILIBRIUM STATE

Yoshitsugu Naka*, Takeshi Omori, Shinnosuke Obi* and Shigeaki Masuda***

*Department of Mechanical Engineering,
Keio University
Yokohama, 223-8522, Japan
obsn@mech.keio.ac.jp

**Chair of Fluid Mechanics and Aerodynamics,
Darmstadt University of Technology
Petersenstr. 30, 64287 Darmstadt, Germany
t.omori@sla.tu-darmstadt.de

ABSTRACT

A novel experimental technique to measure static pressure fluctuation was applied to evaluate velocity-pressure correlation in a turbulent mixing layer. The developing region of the mixing layer was found to be out of equilibrium state, indicating the oscillatory velocity fluctuation due to vortex shedding and remarkable production of turbulence. A simple model for pressure diffusion by Lumley gave satisfactory approximation when the flow approached to the self-similar state. The contribution of pressure-related terms in the transport equation of Reynolds stress is found to be well captured by the present method. The analogy between pressure diffusion and turbulent diffusion becomes weaker when the flow exhibits characteristics which are not found in equilibrium state.

INTRODUCTION

The importance of pressure fluctuation in turbulent flows has long been recognized and is still one of unanswered questions in turbulence research. The correlation of fluctuating pressure and velocity that is originated from large-scale vortex structures plays a significant role in determining the budget of transport equations for turbulence properties. Numerous computational approaches made great contributions to understand the dynamics of the inviscid flow and organized motion of vortices, but it is too complex to give whole description of turbulent motions. Although there are lot of suggestions on close relationships between pressure fluctuation and coherent turbulent fluid motion, the interaction of the velocity and pressure should be explored in various viewpoints.

Problems in the currently available turbulence models lie in the lack of physical characterization of the velocity-pressure correlation, particularly when the turbulence structure departs from equilibrium state. The conditions of flows out of equilibrium state is far from ideal one where calibrations of turbulence models are often undertaken, e.g., isotropic, homogeneous, or simple shear flows. As a consequence, the performance of existing models in predicting complex flows is not well established, unlike the case of simple shear flows. Towards the achievement of better turbulence models for non-equilibrium flows, the key mechanism which is governed by the pressure-related turbulent motions should be addressed.

There are numerous efforts paid for both experimental and computational approaches to understand the role of pressure fluctuation. Relatively few experimental researches about pressure-related statistics are available, mainly because of underlying technical difficulties in measuring static pressure fluctuation at arbitrary location in the flow field. In his pioneering work, Kobashi (1957) combined the condenser microphone with a static pressure tube, and represented a step towards the evaluation of fluctuating pressure. With reference to his work, Shirahama and Toyoda (1993) developed a probe to measure fluctuating pressure with sufficient accuracy in free shear flows. This type of pressure probe enabled a evaluation of fluctuating pressure, for example, Tsuji and Ishihama (2004) introduced this probe to reveal the power-law and proportional constant of normalized pressure spectrum.

The progress of computer technology has enabled the direct numerical simulations (DNS) to be applied to increasingly complex flows with spatial development, which contains remarkably large pressure fluctuation in contrast to simple channel flows, e.g., the transition from turbulent boundary layer along a flat plate to free shear layer, as represented by a DNS study of Yao et al. (2001). A Temporally developing turbulent mixing layer was calculated by Rogers and Moser (1994) and it is indicated that both of the large scale rollers and finer scale ribs play an important role in representing the properties of the shear layer. Nevertheless, both computational and experimental approaches are required to better understand the role of pressure fluctuation in turbulent shear flows.

The present study focuses on the experimental approach to a relatively simple turbulent shear flow but out of equilibrium state of turbulence. A spatially developing turbulent mixing layer is selected for the test case, where the gradual development of oncoming turbulent boundary layer flow to the free shear flow is investigated. A particular attention is paid to the transitional stage of the kinetic energy balance through the non-equilibrium region before the shear layer develops to a self-similar state, as schematically shown in Fig. 1. An advanced technique for simultaneous measurement of velocity and pressure is presented, which is based on our previous work (Omori et al., 2003), and the discussions are made on the existing simple model of pressure-diffusion transport of Reynolds stresses.

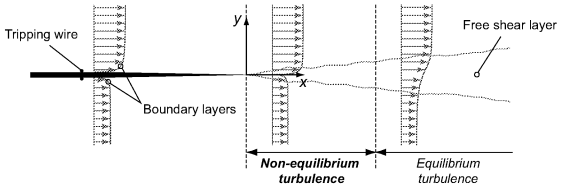

Figure 1: Schematics of the considered flow field.

EXPERIMENTS

Setup and Instruments

The wind tunnel that was specially designed for turbulent mixing layer experiments was used (Omori et al., 2003). The inlet section of the tunnel was divided into two parallel parts, and the fully developed turbulent boundary layers merged at the test section of 0.5m × 0.5m cross section. The orthogonal coordinate system was defined, originating from the trailing edge of the splitter plate, with the x- and y-axes taken in streamwise and transverse directions, respectively, see Fig. 1. The mixing layer was found uniform at least for 70% of the span, corresponding to 10 times of the mixing layer thickness.

The condition of the on-coming inlet boundary layers is summarized in Table 1. All quantities are measured at x=−50mm. Tu_f is the turbulence intensity outside the boundary layer and δ_b stands for the 99% thickness of the boundary layer. The Reynolds number Re is based on the free stream velocity U and the momentum thickness.

A thin static pressure probe, according to Shirahama and Toyoda (1993), was used for the fluctuating pressure measurements, see Fig. 2. The probe was set parallel to the flow direction so that the static pressure fluctuation sensed at the four small holes on the side of the 1.0mm thick pipe was measured. The pressure fluctuation was converted to electric signal by a condenser microphone (RION UC-29) which was mounted on the end of the probe. The performance of the present method was investigated in detail in our preceding work (Omori et al., 2003).

The fluctuating velocity was measured by a hot-wire anemometer (HWA). A commercial X-wires probe (Dantec 55P64) was used for two-component velocity measurements, combined with a constant temperature anemometer (CTA, Kanomax 1011). The microphone and the HWA-probe were mounted on a common traversing unit, so that simultaneous measurements of pressure and two velocity components were possible at arbitrary position. The signal from the CTA and the main amplifier of the microphone were transferred to a PC through a 16bit-A/D converter (National Instruments PCI-MIO-16XE-10). All data acquisition were managed by LabView$^{\mathrm{TM}}$ (National Instruments) and further data processing was handled by programs written on Matlab$^{\mathrm{TM}}$.

A look-up table method by Lueptow et al. (1988) was adopted to convert the signal of X-wires HWA to velocity data. The calibration of the HWA signal was performed by a resolution of 0.3m/s, ranging from 2.5m/s to 6.8m/s; the resolution in direction was 3 degrees, covering from −30 to 30 degrees with respect to the main flow direction. Third-order polynomials were used to fit the curves on the plane composed of a pair of X-wires sensor voltage to obtain velocity variations for arbitrary angle of attack. The resulting look-up table had 80 intervals covering the full range in each sensor voltage, where the desired pair of velocity and angle was sought by use of a bi-linear interpolation function available in the Matlab library.

Table 1: Inlet Conditions

	U [m/s]	Tu_f [%]	δ_b [mm]	Re
high speed side	7.2	0.76	18.8	610
low speed side	3.3	0.94	18.8	260

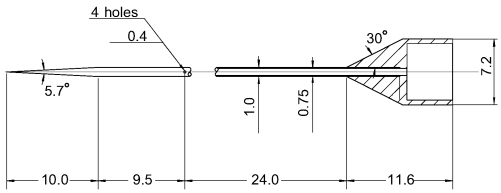

Figure 2: Schematic of the static pressure tube.

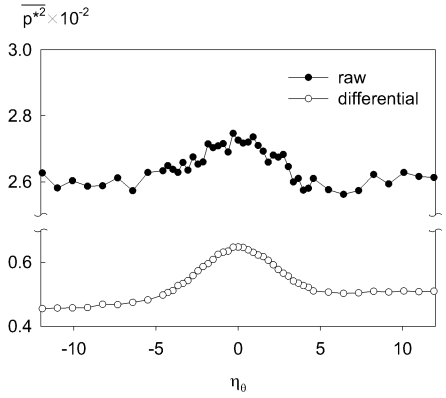

Figure 3: Effect of noise reduction on the fluctuating pressure.

Noise Reduction and Phase Correction Practice

In order to reduce the influence of background noise in wind tunnel, the pressure signal outside the mixing layer was monitored simultaneously by an auxiliary pressure probe which had the identical dimension as that used for the measurement in the shear layer. The signal acquired by the secondary probe was subtracted from that obtained in the shear layer so that only desired local pressure related to turbulent fluid motion could be extracted. The effect of such practice is demonstrated in Fig. 3. The plots after the procedure (differential) show a remarkable reduction of background noze in fluctuating pressure $\overline{p^2}$ in the free stream as compared to the raw data.

Another factor, which contaminates the estimation of velocity-pressure correlation, lies in the phase-lag between velocity and pressure signal. The phase-lag that depends on frequency is caused by the electric circuit of the condenser microphone system. In the present study, an analytical formula is introduced to correct this phase-lag:

$$\theta_d = \pi - \tan^{-1}\left(\frac{1}{2\pi CRf}\right), \qquad (1)$$

where C is electronic capacitance of the condenser microphone, R stands for the input resistance of main amplifier

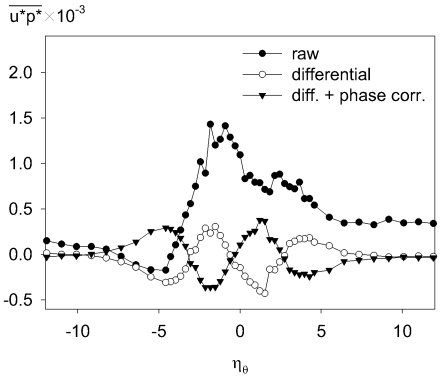

Figure 4: Corrected velocity-pressure correlations.

of the microphone, and f denotes frequency of fluctuating pressure. In the present study, C and R are 6pF and 3GΩ, respectively, according to the hardware specification.

The effect of the correction is demonstrated in Fig. 4; the compensated velocity-pressure correlation shows a profile which takes a sign opposite to that of the value without correction. It is rather surprising that the effect of the correction is not a slight fraction but remarkable in qualitative manner. The results shown hereafter are only those after these correction practices, i.e., differential noise reduction and phase-lag correction.

Interference of Probes

Distance between the X-wires and static pressure tube should be carefully determined so that the interference could be minimized and at the same time the spatial resolution is retained. Based on preliminary experiments, the location for the examination on the effect of the distance between two probes was selected at the location where $\overline{up}$ took maximum across the shear layer. Fig. 5 presents the variation of the second-moment of velocity fluctuation $\overline{u^2}$, pressure fluctuation $\overline{p^2}$, and the correlation $\overline{up}$. Among these, the velocity fluctuation is most sensitive to the probe distance, presumably due to the change of the flow field near the X-wires probe caused by the blockage of pressure tube. On the other hand, the pressure fluctuation is less sensitive to the probe distance. The correlation between the velocity and pressure is small in magnitude. Although there is a slight variation, the dependence of this quantity to the probe distance is not clearly addressed because of measurement accuracy. Based on these results, the probe distance Δh was set to 2.0mm where the velocity fluctuation is nearly unaffected.

Data processing

The statistics were calculated from 80,000 samples. The sampling rate of 4kHz was selected to evaluate quantities that require high temporal resolution, such as energy spectra and derivatives with respect to the time. For other statistics the sampling rate was fixed to 200Hz which was found sufficiently high from the examination of auto-correlation of velocity fluctuation. The resulting integration time was 400 seconds for turbulence statistics. Typically, it took about an hour by a PC (Pentium4 2.8GHz) to complete a post-processing of each measurement to draw a profile, comprising 48 points, across the mixing layer.

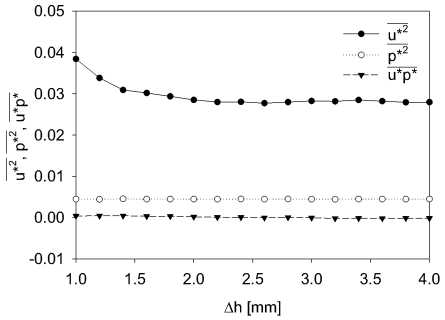

Figure 5: Influence of the probe distance.

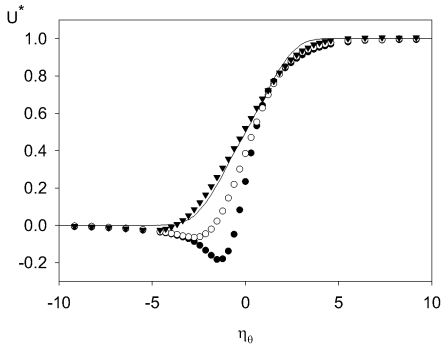

Figure 6: Profile of the streamwise mean velocity; Symbols • : $x = 25$ mm, ∘ : $x = 50$ mm, ▼ : $x = 100$ mm, —— : DNS result of Rogers and Moser (1994)

RESULTS

Primary Remarks

The velocity profiles across the shear layer are measured at three different streamwise locations, x=25mm, 50mm and 100mm. The development of the shear layer thickness, δ, was examined by means of the expansion factor of free shear layer, $S = (U_c/U_s)(\Delta\delta/\Delta x)$ (Pope, 2000), with U_c being the convective velocity defined by $U_c = (U_h + U_l)/2$ where U_h and U_l are the free stream velocity of higher and lower velocity side, respectively, and U_s is the velocity difference, $U_s = U_h - U_l$. The value of S slightly decreases from 0.089, which is evaluated at the interval between 25mm $\leq x \leq$ 50mm, down to 0.086 at 50mm $\leq x \leq$ 100mm. The variation of S indicates that the shear layer is still under the development state.

Statistics of Non-Equilibrium Turbulent Mixing Layer

The streamwise mean velocity profiles are shown in Fig. 6. The velocity U^* is normalized by the velocity difference U_s ($U^* = (U - U_l)/U_s$), and the non-dimensional coordinate η_θ is calculated using the momentum thickness of the shear layer at $x = 100$mm ($\eta_\theta = y/\theta_d$). The wake of the splitter plate is observed at all locations in contrast to the profile of DNS by Rogers and Moser (1994) representing the self-similar state. The deficit in the velocity profile reaches $0.18U_s$ at $x = 25$mm; it decreases down to $0.07U_s$ at 50mm and still persists in the most downstream location, providing a slight under-shoot of the lower velocity side by $0.02U_s$ at $x = 100$mm.

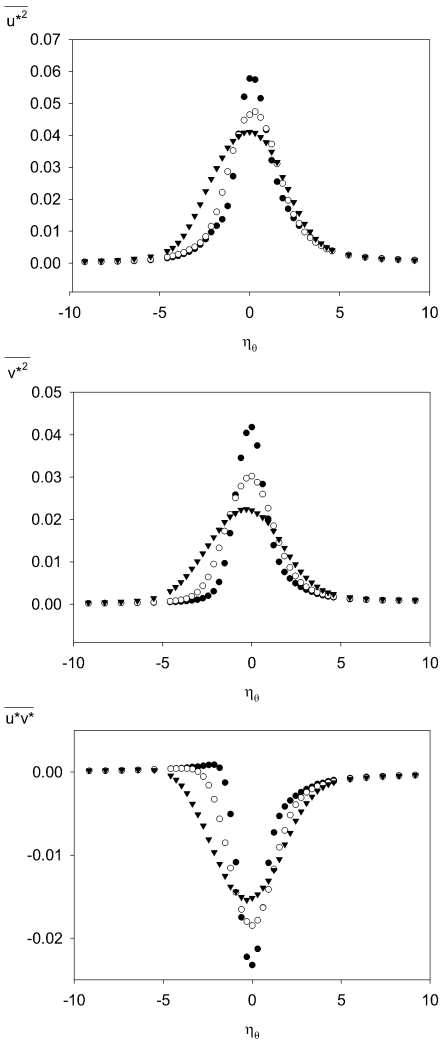

Figure 7: Components of Reynolds stress tensor; (a) $\overline{u^2}$, (b) $\overline{v^2}$, (c) $\overline{uv}$; Symbols ● : $x = 25$ mm, ○ : $x = 50$ mm, ▼ : $x = 100$ mm

Figure 7 presents the profiles of the individual Reynolds stress component at the same location as for Fig. 6. It is shown that every component decreases in downstream, with the $\overline{v^2}$-component indicates a slightly faster decrease when compared to the others. As the shear layer spreads to the direction of lower velocity side (negative η_θ), the distribution becomes broader for the all components. It is worth to notice that the shear stress $\overline{uv}$ changes the sign in a narrow region in accordance with the mean velocity distribution that exhibits a distinct wake shape.

The flow characteristics are further explored by means of the power spectrum density of normal velocity component v, see Fig. 8, evaluated at the center of the shear layer, i.e., $\eta_\theta = 0$. At the most upstream location, the distribution shows a peak near 330Hz which corresponds to $St = 0.083$, with St being the Strouhal number based on the thickness of the splitter plate and U_s. Weaker peaks are also observed near 260Hz and 160Hz at $x = 50$mm and 100mm, respectively.

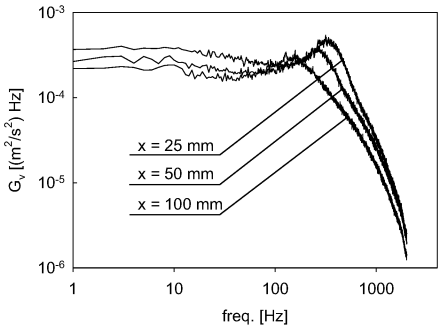

Figure 8: Power Spectrum of v.

The characteristic frequency shown by the spectra is an indication of vortex shedding at a constant frequency, and the observed gradual decrease of the characteristic frequency is likely due to the consequence of vortex merging which occurs in the development stage. The DNS by Yao et al. (2001) reports a remarkable vortex shedding in the wake of a blunt body, with the Strouhal number 0.118 evaluated right behind the plate. When the above-mentioned streamwise variation of the characteristic frequency is taken into account, it is fair to consider that the periodic vortex shedding also exists in the present study especially near the trailing edge of the splitter plate. The influence of the vortex shedding gradually decays as the flow approaches to the self-similar state.

Velocity-Pressure Correlation in the Shear Layer

Figure 9 shows the velocity-pressure correlations $\overline{up}$ and $\overline{vp}$, which are directly measured by the present method, comparing with those evaluated by Lumley's model (1978) based on the triple-velocity correlation at the three streamwise locations:

$$\overline{up} = -\frac{1}{5}\left(\overline{u^3} + \overline{uv^2}\right), \quad (2)$$

$$\overline{vp} = -\frac{1}{5}\left(\overline{u^2 v} + \overline{v^3}\right). \quad (3)$$

It is shown that both $\overline{up}$ and $\overline{vp}$ significantly vary across the shear layer, changing their sign at the center, and $\overline{up}$ consistently exceeds $\overline{vp}$ in magnitude. The gradual decay of all quantities is also observed in downstream when comparing (a), (b) and (c).

Lumley's model provides relatively fair agreement for both components at locations shown in Fig. 9 (b) and (c). An obvious departure is, however, evident in Fig. 9(a) that is measured at the most upstream location, where Lumley's model yields an opposite sign to $\overline{up}$ and the magnitude of $\overline{vp}$ is over-estimated. These disagreements may be related to the existence of the characteristic frequency in the power density of the velocity fluctuation v, see Fig. 8.

DISCUSSION

The significance of the velocity pressure correlation is further investigated in terms of the transport equation of Reynolds stress:

$$\frac{D\overline{u_i u_j}}{Dt} = P_{ij} - (D^t_{ij} + D^p_{ij} + D^\nu_{ij}) + \Phi_{ij} - \varepsilon_{ij}, \quad (4)$$

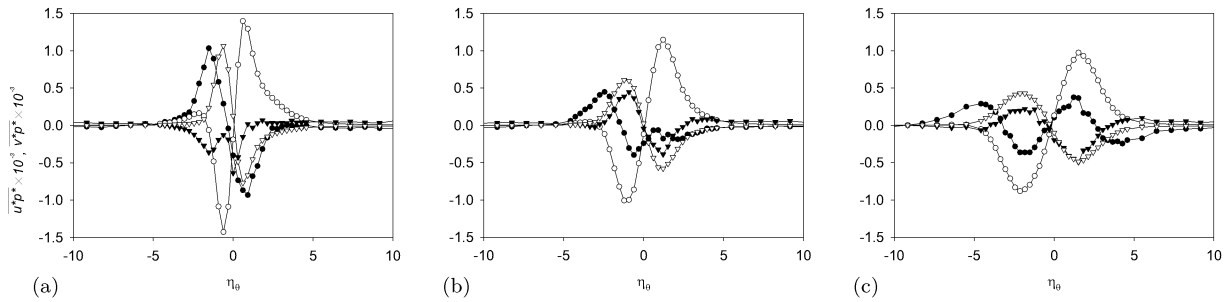

Figure 9: Profiles of $\overline{up}$ and $\overline{vp}$; (a) $x = 25$ mm, (b) $x = 50$ mm, (c) $x = 100$ mm; Symbols $\bullet : \overline{up}$, $\circ : \overline{up}$ (Lumley model), $\blacktriangledown : \overline{vp}$, $\triangledown : \overline{vp}$ (Lumley model)

where the terms on the right hand side, P_{ij}, D_{ij}, Φ_{ij}, and ε_{ij} represent production, diffusion, re-distribution and dissipation of the Reynolds stress $\overline{u_i u_j}$. Among the three diffusion transports, the molecular viscous transport D^{ν}_{ij} may be neglected because of large Reynolds number; the other two, i.e., the turbulent diffusion D^{t}_{ij} and the pressure diffusion D^{p}_{ij}, are of primary concern and discussed subsequently. Table 2 summarizes some representative terms in the equation which are evaluated in the present study. Because of the restriction of the available quantities, only the terms on the right column of the table are evaluated. Also note that Taylor's hypothesis is applied to the estimation of the re-distribution term in the equation for the $\overline{u^2}$-component, with $\hat{u}$ being the instantaneous streamwise velocity component.

Figure 10 presents the distribution of production and the re-distribution term in the $\overline{u^2}$-equation at three streamwise locations. The DNS result of Rogers and Moser (1994) are shown for reference to the equilibrium state. It is seen that the production rate far exceeds the re-distribution at $x = 25$mm, though rapidly decreases in downstream. At the most downstream location, $x = 100$mm in (c), the measured values well coincide with DNS result. It is found that the evaluated re-distribution term is consistently smaller than the production in magnitude. It should be noted that there is a narrow region, $-3 \leq \eta_\theta \leq -1$ at $x = 25$mm (a), where the production and re-distribution show opposite sign.

The balance of the representative terms are also presented for the $\overline{uv}$- and $\overline{v^2}$-components in Figs. 11 and 12, respectively. For both components, the production P_{ij}, turbulent diffusion D^{t}_{ij} and pressure diffusion D^{p}_{ij} are compared. Similarly to the case in $\overline{u^2}$-component, the production term is over-proportional to the others at the most upstream location, x=25mm, and rapidly decreases in downstream. In particular, the production of $\overline{v^2}$, Fig. 12(a), exhibits remarkable magnitude, which is not the case for the self-similar state where the production P_{22} nearly vanishes.

The two diffusion terms, turbulent- and pressure-diffusion, of these two components indicate reasonable proportion: They are opposite in sign and the turbulent diffusion is consistently larger than its counterpart across the shear layer. Again, the situation at the most upstream location, x=25mm in Fig. 12, is a little different from the other two downstream locations, where the analogy between the turbulent- and pressure-diffusion is not likely to hold.

The above discussion points to the fact that the relatively simple approximation of the pressure diffusion by Lumley (1978) well represents the simple shear flow close to the self-similar state. However, the analogy between the turbulent- and pressure-diffusion gradually breaks down as the flow starts to exhibit certain characteristics such as the existence of vortex shedding, or the departure from equilibrium state. The role of pressure fluctuation becomes more important as the complexity of turbulence structure increases.

Table 2: Terms of Reynolds Stress Equation.

	exact form	present form
P_{11}	$-2\rho\left(\overline{u^2}\dfrac{\partial U}{\partial x}+\overline{uv}\dfrac{\partial U}{\partial y}\right)$	$-2\rho\overline{uv}\dfrac{\partial U}{\partial y}$
Φ_{11}	$2p\overline{\dfrac{\partial u}{\partial x}}$	$-2p\overline{\dfrac{du}{dt}\dfrac{1}{\hat{u}}}$
P_{12}	$-\rho\left(\overline{u^2}\dfrac{\partial V}{\partial x}+\overline{v^2}\dfrac{\partial U}{\partial y}\right)$	$-\rho\overline{v^2}\dfrac{\partial U}{\partial y}$
D^{t}_{12}	$-\rho\left(\dfrac{\partial\overline{u^2v}}{\partial x}+\dfrac{\partial\overline{uv^2}}{\partial y}\right)$	$-\rho\dfrac{\partial\overline{uv^2}}{\partial y}$
D^{p}_{12}	$-\left(\dfrac{\partial\overline{pv}}{\partial x}+\dfrac{\partial\overline{pu}}{\partial y}\right)$	$-\dfrac{\partial\overline{pu}}{\partial y}$
P_{22}	$-2\rho\left(\overline{vu}\dfrac{\partial V}{\partial x}+\overline{v^2}\dfrac{\partial V}{\partial y}\right)$	$-2\rho\overline{v^2}\dfrac{\partial V}{\partial y}$
D^{t}_{22}	$-\rho\left(\dfrac{\partial\overline{u^3}}{\partial x}+\dfrac{\partial\overline{u^2v}}{\partial y}\right)$	$-\rho\dfrac{\partial\overline{u^2v}}{\partial y}$
D^{p}_{22}	$-2\dfrac{\partial\overline{pv}}{\partial y}$	$-2\dfrac{\partial\overline{pv}}{\partial y}$

CONCLUDING REMARKS

The experimental evaluation of the pressure-related turbulence statistics has been undertaken in a free mixing layer out of equilibrium state. The noise reduction as well as phase-lag correction procedure is shown to be successful in evaluating the fluctuating pressure and the correlation between velocity and pressure. The distance between the pressure probe and X-wires has been carefully adjusted to minimize the interference and at the same time to retain the spatial resolution.

The characteristics of spatial developing turbulent mixing layer were investigated with particular focused on the pressure-related quantities. Fundamental statistics are presented, and it is indicated that the flow characteristics are under the development, showing remarkable velocity oscil-

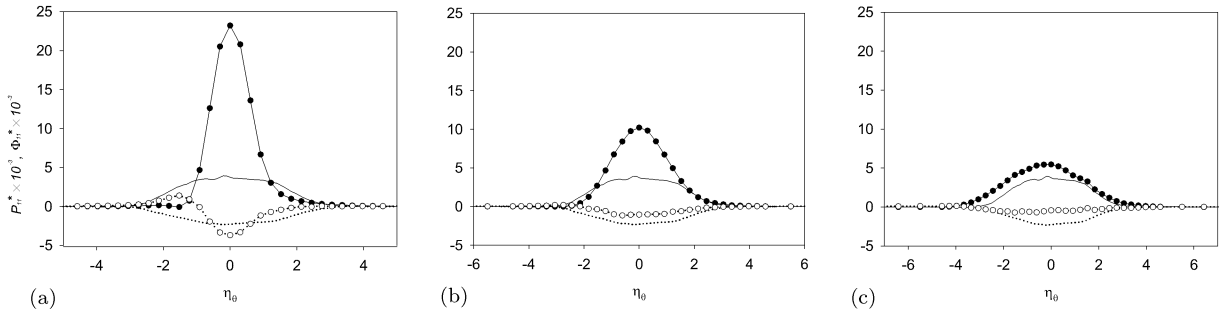

Figure 10: Estimated re-distribution Φ_{11}; (a) $x = 25$ mm, (b) $x = 50$ mm, (c) $x = 100$ mm; Symbols $\bullet$: P_{11}, $\circ$: Φ_{11}, ——: P_{11} (DNS), $\cdots\cdots$: Φ_{11} (DNS), DNS data of Rogers & Moser (1994)

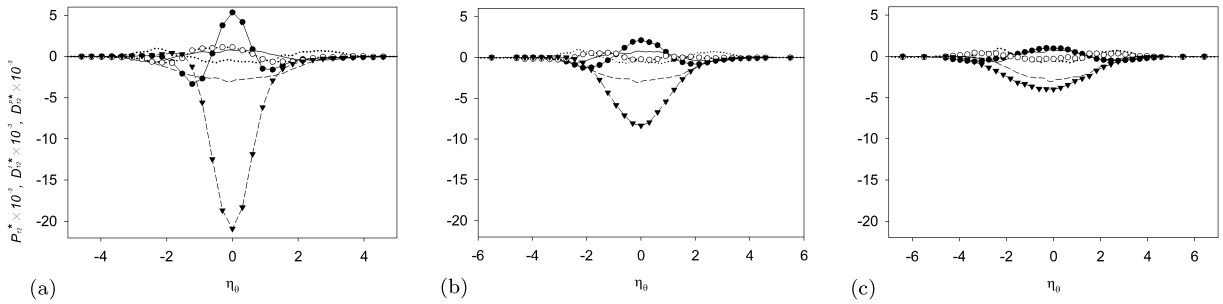

Figure 11: Estimated turbulent-diffusion D^t_{12} and pressure-diffusion D^p_{12}; (a) $x = 25$ mm, (b) $x = 50$ mm, (c) $x = 100$ mm; Symbols $\bullet$: D^t_{12}, $\circ$: D^p_{12}, $\blacktriangledown$: P_{12}, —— : D^t_{12} (DNS), $\cdots\cdots$: D^p_{12} (DNS), - - - - - : P_{12} (DNS)

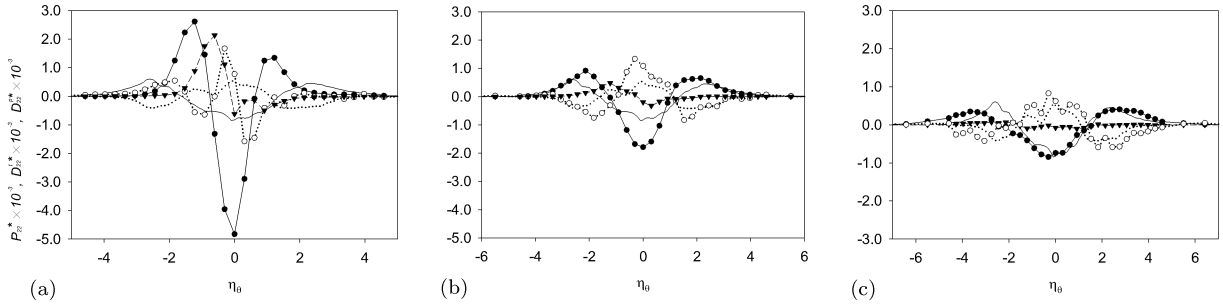

Figure 12: Estimated turbulent-diffusion D^t_{22} and pressure-diffusion D^p_{22}; (a) $x = 25$ mm, (b) $x = 50$ mm, (c) $x = 100$ mm; Symbols $\bullet$: D^t_{22}, $\circ$: D^p_{22}, $\blacktriangledown$: P_{22}, —— : D^t_{22} (DNS), $\cdots\cdots$: D^p_{22} (DNS)

lation inherent to vortex shedding from the splitter plate. Velocity-pressure correlations are directly measured and compared with Lumley's model. The budget of Reynolds stress transport equation is examined, and the measured pressure-related terms showed fair agreement with available DNS data. The analogy between the turbulent diffusion and pressure diffusion does not seem to hold in the region where the turbulence structure departs from that in the energy equilibrium state.

REFERENCES

Bell, J. H., and Mehta., R. D., 1990, "Development of a two-stream mixing layer from tripped and untripped boundary layers" *AIAA J.*, 28-12, 2034-2042.

Kobashi, Y., 1957, "Measurement of pressure fluctuation in the wake of cylinder", *J. Phys. Soc. Jpn*, 12-5, 533

Lueptow, R. M., Breuer, K. S., and Haritonidis, J. H., 1988, "Computer-aided calibration of X-probes using a look-up table", *Exp. Fluids*, 6, 115-118.

Lumley, J. L., 1978, "Computational modeling of turbulent flows", *Advances in Applied Mechanics* 18, 123-176.

Omori, T., Obi, S., and Masuda, S., 2003, "Experimental study on velocity-pressure correlation in turbulent mixing layer," *Turbulence, Heat and Mass transfer 4*, K. Hanjalić et al., eds., Begell House Inc., 253-260.

Pope, S. B., 2000, *Turbulent Flows*, Cambridge University Press.

Rogers, M. M., and Moser, R. D., 1994, "Direct simulation of a self similar turbulent mixing layer", *Phys. Fluids*, 6 (2), 903-922.

Shirahama, Y., and Toyoda, K., 1993, "Development of the probe to measure static-pressure fluctuations", *Trans. JSME, Series B*, Vol. 59-567, 3381-3387, in Japanese.

Tsuji, Y., and Ishihama, T., 2003, "Similarity scaling of pressure fluctuation in turbulence", *Phys. Rev. E*, 68, 026309.

Yao, Y. F., Thomas, T. G., Sandham, N. D., and Williams, J. J. R., 2001, "Direct numerical simulation of turbulent flow over a rectangular trailing edge", *Theo. Comp. Fluid Dynamics*, 14, 337-358.